Transition from radiatively inefficient to cooling dominated phase in two temperature accretion discs around black holes

Monika Sinha, S. R. Rajesh and Banibrata Mukhopadhyay

Astronomy and Astrophysics Program, Department of Physics, Indian Institute of Science, Bangalore 560012, India; *msinha@physics.iisc.ernet.in, rajesh@physics.iisc.ernet.in, bm@physics.iisc.ernet.in*

Abstract We investigate the transition of a radiatively inefficient phase of a viscous two temperature accreting flow to a cooling dominated phase and vice versa around black holes. Based on a global sub-Keplerian accretion disc model in steady state, including explicit cooling processes self-consistently, we show that general advective accretion flow passes through various phases during its infall towards a black hole. Bremsstrahlung, synchrotron and inverse Comptonization of soft photons are considered as possible cooling mechanisms. Hence the flow governs a much lower electron temperature $\sim 10^8 - 10^{9.5}$K compared to the hot protons of temperature $\sim 10^{10.2} - 10^{11.8}$K in the range of the accretion rate in Eddington units $0.01 \lesssim \dot{M} \lesssim 100$. Therefore, the solutions may potentially explain the hard X-rays and the γ-rays emitted from AGNs and X-ray binaries. We finally compare the solutions for two different regimes of viscosity and conclude that a weakly viscous flow is expected to be cooling dominated compared to its highly viscous counterpart which is radiatively inefficient. The flow is successfully able to reproduce the observed luminosities of the under-fed AGNs and quasars (e.g. Sgr A^*), ultra-luminous X-ray sources (e.g. SS433), as well as the highly luminous AGNs and ultra-luminous quasars (e.g. PKS 0743-67) at different combinations of the mass accretion rate and ratio of specific heats.

Key words: accretion, accretion disc, black hole physics, hydrodynamics, radiative transfer

1 INTRODUCTION

The observed hard X-rays from, e.g., Cyg X-1 can not be explained (Lightman & Shapiro 1975) by the model of cool Keplerian accretion disc (Pringle & Rees 1972; Shakura & Sunyaev 1973; Novikov & Thorne 1973). Indeed Eardley & Lightman (1975) found that a Keplerian disc is unstable due to thermal and viscous effects with constant viscosity parameter α (Shakura & Sunyaev 1973) which was later shown by Eggum, Coroniti & Katz (1985) by numerical simulations. Since then, the idea of two component accretion disc started floating around. For example, Muchotrzeb & Paczyński (1982) introduced the idea of sub-Keplerian, transonic accretion, which was later improved by other authors (Chakrabarti 1989, 1996; Mukhopadhyay 2003).

Shapiro, Lightman & Eardley (1976) introduced a two temperature Keplerian accretion disc at a low mass accretion rate which is significantly hotter than the single temperature Keplerian disc of Shakura & Sunyaev (1973). Various states of Cyg X-1 could be well explained by this model (e.g. Melia & Misra 1993). However, in this model, solutions appear thermally unstable. Narayan & Popham (1993) and subsequently Narayan & Yi (1995) introduced advection to stabilize the system. However, this model, with inefficient cooling mechanisms, could explain only a particular class of hot systems. Moreover, the model kept the electron heating decoupled from the disc hydrodynamics. On the other hand, Chakrabarti & Titarchuk

(1995) and later Mandal & Chakrabarti (2005) modeled similar kind of flows emphasizing possible formation of shock and its consequences therein. However, they also did not consider the effect of electron heating self-consistently into the hydrodynamic equation, and thus the hydrodynamic quantities remain decoupled from the rate of electron heating.

In the present paper, we model a self-consistent accretion disc in two temperature transonic sub-Keplerian regime. Considering all the hydrodynamic equations of the disc along with thermal components we solve the coupled set of equations self-consistently. We investigate switching over the flow during infall, from the radiatively inefficient nature, e.g. ADAF (Narayan & Yi 1994), to general advective paradigm and then to cooling dominated phase and vice versa. In order to apply the model to explain observations, we focus on the ultra-luminous X-ray (ULX) sources (e.g. SS433), under-luminous AGNs and quasars (e.g. Sgr A^*) and ultra-luminous quasars and highly luminous AGNs (e.g. PKS 0743-67), while the first set of objects is likely to be the "radiation trapped" accretion disc.

In the next section, we discuss the model equations governing the system and the procedure to solve them. In §3 and §4, we describe the two temperature accretion disc around stellar mass and supermassive black holes respectively. Section 5 compares the disc flow of low Shakura-Sunyaev (1973) α with that of high α. Then we summarize the results in §6 with implications.

2 FORMALISM

We set five coupled differential equations to describe the laws of conservation in the sub-Keplerian advective accretion disc, which is presumably optically thin. All the variables are expressed throughout in dimensionless units, unless stated otherwise. The radial velocity v and sound speed c_s are expressed in units of light speed c, the specific angular momentum λ in GM/c, where G is the Newton's gravitational constant and M is the mass of the black hole, expressed in units of solar mass $M_\odot$, the radial coordinate x in units of GM/c^2, the density ρ and the total pressure P accordingly. The disc fluid, which behaves as an (almost) noninteracting gas, consists of ions and electrons, apart from radiation.

2.1 Conservation laws

(a) Mass transfer:

$$\frac{1}{x}\frac{\partial}{\partial x}(x\rho v) = 0, \text{ and thus } \dot{M} = -4\pi x\Sigma v, \tag{1}$$

where the surface density

$$\Sigma = I_n\,\rho_{eq}\,h(x), \; I_n = (2^n n!)^2/(2n+1)! \text{ (Matsumoto et al. 1984)}, \tag{2}$$

ρ_{eq} is density at the equatorial plane, half-thickness of the disc

$$h(x) = c_s x^{1/2} F^{-1/2}, \tag{3}$$

F is the magnitude of gravitational force.

(b) Radial momentum balance:

$$v\frac{dv}{dx} + \frac{1}{\rho}\frac{dP}{dx} - \frac{\lambda^2}{x^3} + F = 0 \tag{4}$$

when following Mukhopadhyay (2002) the gravitational force corresponding to the pseudo-Newtonian potential

$$F = \frac{(x^2 - 2a\sqrt{x} + a^2)^2}{x^3[\sqrt{x}(x-2) + a]^2}, \tag{5}$$

where a is the Kerr parameter, which, for simplicity, is chosen to be zero (Schwarzschild black hole) for the present purpose. Following Ghosh & Mukhopadhyay (2009), we also define

$$\beta = \frac{\text{gas pressure } P_{gas}}{\text{total pressure } P} = \frac{6\gamma - 8}{3(\gamma - 1)} \tag{6}$$

where γ is the ratio of specific heats given by $4/3 \leq \gamma \leq 5/3$, $P_{gas} = P_i$ (ion pressure) + P_e (electron pressure), such that

$$P = \frac{\rho}{\beta\,c^2}\left(\frac{kT_i}{\mu_i m_i} + \frac{kT_e}{\mu_e m_i}\right) = \rho c_s^2, \tag{7}$$

where T_i, T_e are respectively the ion and electron temperatures in Kelvin, m_i is the mass of a proton in gm, μ_i and μ_e respectively are the corresponding effective molecular weight, k the Boltzmann constant. Note that for $\gamma = 4/3$, $\beta = 0$; pure radiation flow, and for $\gamma = 5/3$, $\beta = 1$; pure gas flow.

(c) Azimuthal momentum balance:

$$v\frac{d\lambda}{dx} = \frac{1}{\Sigma x}\frac{d}{dx}\left(x^2|W_{x\phi}|\right), \tag{8}$$

where following Mukhopadhyay & Ghosh (2003) the shearing stress is given by

$$W_{x\phi} = -\alpha\left(I_{n+1}P_{eq} + I_n v^2 \rho_{eq}\right)h(x), \tag{9}$$

where α is the dimensionless viscosity parameter and P_{eq} and ρ_{eq} are the pressure and density respectively at the equatorial plane which will be assumed to be the same as general P and ρ respectively in obtaining solutions.

(d) Energy production rate:

$$\frac{vh(x)}{\Gamma_3 - 1}\left(\frac{dP}{dx} - \Gamma_1\frac{P}{\rho}\frac{d\rho}{dx}\right) = Q^+ - Q_{ie}, \tag{10}$$

where following Mukhopadhyay & Ghosh (2003) the heat generated by viscous dissipation

$$Q^+ = \alpha(I_{n+1}P + I_n v^2 \rho)h(x)\frac{d\lambda}{dx}, \tag{11}$$

when the Coulomb coupling, written in dimensionless form (Bisnovatyi-Kogan & Lovelace 2000) Q_{ie} is given in the dimensionful unit as

$$q_{ie} = \frac{8(2\pi)^{1/2}e^4 n_i n_e}{m_i m_e}\left(\frac{T_e}{m_e} + \frac{T_i}{m_i}\right)^{-3/2}\ln(\Lambda)\,(T_i - T_e)\ \mathrm{erg/cm^3/sec}, \tag{12}$$

where n_i and n_e respectively denote number densities of ion and electron, e the electron charge, $\ln(\Lambda)$ the Coulomb logarithm. We also define

$$\Gamma_3 = 1 + \frac{\Gamma_1 - \beta}{4 - 3\beta}, \tag{13}$$

$$\Gamma_1 = \beta + \frac{(4 - 3\beta)^2(\gamma - 1)}{\beta + 12(\gamma - 1)(1 - \beta)}. \tag{14}$$

(e) Energy radiation rate:

$$\frac{vh(x)}{\Gamma_3 - 1}\left(\frac{dP_e}{dx} - \Gamma_1\frac{P_e}{\rho}\frac{d\rho}{dx}\right) = Q_{ie} - Q^-, \tag{15}$$

where the total heat radiated away (Q^-) by the bremsstrahlung (q_{br}), synchrotron (q_{syn}) processes and inverse Comptonization (q_{comp}) due to soft synchrotron photons is given in dimensionful form as (Narayan & Yi 1995; Mandal & Chakrabarti 2005)

$$q^- = q_{br} + q_{syn} + q_{comp}, \tag{16}$$

where

$$q_{br} = 1.4 \times 10^{-27}\, n_e\, n_i T_e^{1/2} \left(1 + 4.4 \times 10^{-10} T_e\right)\ \text{erg/cm}^3/\text{sec},$$

$$q_{syn} = \frac{2\pi}{3c^2} kT_e\, \frac{\nu_a^3}{R}\ \text{erg/cm}^3/\text{sec},\ \ R = x\, GM/c^2,$$

$$q_{comp} = \mathcal{F}\, q_{syn},\ \ \mathcal{F} = \eta_1 \left(1 - \left(\frac{x_a}{3\theta_e}\right)^{\eta_2}\right),\ \ \eta_1 = \frac{p(A-1)}{(1-pA)},\ \ p = 1 - \exp(-\tau_{es}),$$

$$A = 1 + 4\theta_e + 16\theta_e^2,\ \ \theta_e = kT_e/m_e c^2,\ \ \eta_2 = -1 - \frac{ln(p)}{ln(A)},\ \ x_a = h\nu_a/m_e c^2, \qquad (17)$$

when τ_{es} is the scattering optical depth given by

$$\tau_{es} = \kappa_{es}\rho\, h \qquad (18)$$

where $\kappa_{es} = 0.38\ \text{cm}^2/\text{gm}$ and ν_a is the synchrotron self-absorption cut off frequency. However, the total optical depth should include the effects of absorption due to nonthermal processes. Therefore, effective optical depth is given by

$$\tau_{eff} \simeq \sqrt{\tau_{es}\, \tau_{abs}} \qquad (19)$$

where approximately $\tau_{abs} \simeq 6 \times 10^{23}\, \rho^2\, T_e^{-7/2}\, h$.

Now, combining all the equations we obtain

$$\frac{dv}{dx} = \frac{N(x, v, \lambda, c_s, T_e)}{D(v, c_s)}, \qquad (20)$$

where

$$N = \frac{\Gamma_1 + 1}{\Gamma_3 - 1} v^2 c_s J - \frac{\alpha^2 c_s}{x} H \left(\frac{I_{n+1}}{I_n} c_s^2 + v^2\right) - \alpha^2 \frac{I_{n+1}}{I_n} 2HJ + \frac{\Gamma_1 - 1}{\Gamma_3 - 1} v^2 c_s^3 G + \alpha H \left(\frac{2\lambda v c_s}{x^2}\right)$$
$$+ \frac{4\pi Q_{ie}}{\dot{M}} v^2 c_s^2 x^{3/2} F^{-1/2}, \qquad (21)$$

$$D = \frac{1 - \Gamma_1}{\Gamma_3 - 1} c_s^3 v + 2\alpha c_s \frac{I_{n+1}}{I_n} H \left(\frac{c_s^2}{v} - v\right) + \frac{\Gamma_1 + 1}{\Gamma_3 - 1} v^2 c_s^2 \left(v - \frac{c_s^2}{v}\right) + \alpha^2 v H \left(\frac{H}{v}\right) \qquad (22)$$

and

$$G = \left(\frac{3}{2x} - \frac{1}{2F}\frac{dF}{dx}\right),\ \ H = \left(I_{n+1}c_s^2 + I_n v^2\right),\ \ J = \left(c_s^2 G + \frac{\lambda^2}{x^3} - F\right). \qquad (23)$$

Finally combining eqns. (4), (8) and (15) we obtain

$$\frac{dc_s}{dx} = \left(\frac{c_s}{v} - \frac{v}{c_s}\right)\frac{dv}{dx} + \frac{J}{c_s}, \qquad (24)$$

$$\frac{d\lambda}{dx} = \left(\frac{2\alpha x}{v c_s}\frac{I_{n+1}}{I_n}\left(\frac{c_s^3}{v} - v c_s\right) + \alpha x\right)\frac{dv}{dx} + \left(\frac{c_s^2 - 2x\alpha J}{c_s} + v\right), \qquad (25)$$

$$\frac{dT_e}{dx} = (1 - \Gamma_1)T_e \frac{v}{c_s^2}\frac{dv}{dx} + (1 - \Gamma_1)T_e \left(\frac{J}{c_s^2} + G\right) + \frac{(\Gamma_3 - 1)4\pi}{\dot{M}}\frac{c_s x^{3/2}}{F^{1/2}}\left(Q^{ie} - Q^-\right). \qquad (26)$$

Now following the procedure adopted in the previous works (e.g. Chakrabarti 1996, Mukhopadhyay 2003, Mukhopadhyay & Ghosh 2003) we solve eqns. (20), (24), (25), (26) for v, c_s, λ, T_e.

There is a possibility of convective instability in advective flows as the entropy increases inwards (e.g. Narayan & Yi 1994, Chakrabarti 1996). This may help in explaining transport as well, as proposed by Narayan & Yi (1994). When the square of effective frequency

$$\nu_{eff}^2 = \nu_{\mathrm{BV}}^2 + \nu_r^2 < 0 \tag{27}$$

dynamical convective instability arises, where ν_{BV} is the Brunt-Väisälä frequency and ν_r the radial epicyclic frequency given by

$$\nu_{\mathrm{BV}}^2 = -\frac{1}{\rho}\frac{dP}{dx}\frac{d}{dx}ln\left(\frac{P^{1/\gamma}}{\rho}\right), \quad \nu_r^2 = \frac{2\lambda}{x^3}\frac{d\lambda}{dx}. \tag{28}$$

2.2 Solution procedure

As previous works (e.g. Chakrabarti 1996, Mukhopadhyay 2003, Mukhopadhyay & Ghosh 2003), in order to obtain the steady state solution we primarily need to find out the self-consistent value of the sonic/critical radius x_c and the corresponding specific angular momentum λ_c of the flow. For the present purpose of a two temperature flow, at x_c the electron temperature T_{ec} also needs to be specified. Note that the set of values x_c, λ_c, T_{ec} has to be adjusted appropriately to obtain self-consistent solution connecting the outer boundary to the black hole event horizon through x_c. Depending on the type of accreting system to model, we then have to specify the related inputs: $\dot{M}$, M and γ. Importantly, unlike former works (e.g. Chakrabarti & Titarchuk 1995, Chakrabarti 1996, Mukhopadhyay & Ghosh 2003) here x_c changes with the change of $\dot{M}$, which is very natural because the various cooling processes considered here explicitly depend on $\dot{M}$. Finally, we have to solve the Eqn. (20) from x_c to the black hole event horizon, and then outwards upto the transition radius x_o where the disc deviates from the Keplerian to the sub-Keplerian regime such that $\lambda/\lambda_K = 1$ (λ_K being the specific angular momentum of the Keplerian part of the disc).

3 DISC FLOWS AROUND STELLAR MASS BLACK HOLES

We concentrate on the super-Eddington accretor which presumably is the case of ultra-luminous X-ray binaries. We mainly intend to understand the explicit dependence of the disc properties on the cooling processes and then the variation of the cooling efficiency f with the disc radii. Note that f is defined to be the ratio of the energy advected by the flow to the energy dissipated; $f \to 1$ for the advection dominated accretion flow (in short ADAF; Narayan & Yi 1994, 1995) and $f < 1$ for the general advective accretion flow (in short GAAF; Chakrabarti 1996, Mukhopadhyay 2003, Mukhopadhyay & Ghosh 2003). Far away from the black hole the disc becomes (or tends to become) of one temperature when the gravitational power is weaker and hence the angular momentum profile remains Keplerian in the presence of efficient cooling.

Note that the "radiation trapped" accretion disc can be attributed to the radiatively driven outflow and jet which is likely to occur when the accretion rate is super-Eddington (Lovelace, Romanova & Newman 1994, Begelman, King & Pringle 2006, Fabbiano 2004, Ghosh & Mukhopadhyay 2009), as seen in the ULX sources such as SS433 (with luminosity $\sim 10^{40}$ erg/s or so; Fabrika 2004). In order to describe such sources, we consider $\dot{M} = 10$. Throughout we express $\dot{M}$ in units of Eddington limit. The set of input parameters used for this case is given in Table 1. However, a detailed work of the two temperature viscous accretion flows in the possible range of accretion rates: $0.01 \lesssim \dot{M} \lesssim 100$, around rotating stellar mass black holes is under preparation (Rajesh & Mukhopadhyay 2009)

A high mass accretion rate renders density to be very high which is very favourable for various cooling mechanisms. Naturally this results in f being low which finally affects the two temperature nature. The profile of velocity shown in Fig. 1a clearly indicates a centrifugal barrier at around $x \sim 30$. However, further out, at $x \sim 50$, f increases (see Fig. 1c) as the energy radiated due to the bremsstrahlung process is weaker than the energy transferred from protons to electrons through the Coulomb coupling (see Fig. 2). Subsequently, the synchrotron process becomes dominant (see Fig. 2), causing $f \to 0$. However, the presence of strong advection near the black hole does not allow the flow to radiate efficiently rendering $f \to 1$ again. This also leads to marginal convective instability only at $x < 10$, as is evident from Fig. 1d (see, however, Narayan, Igumenshchev & Abramowicz 2000, Quataert & Gruzinov 2000).

Figure 2 shows the variation of cooling processes and the corresponding temperature profiles with the radial coordinate. At the transition radius the disc remains of one temperature (see Fig. 2). However, a strong two temperature nature appears when the flow advances with a sub-Keplerian angular momentum. This is because far away the electrons and ions are in thermal equilibrium, around the transition radius, particularly at a high $\dot{M}$. As matter infalls through the sub-Keplerian regime, the ions become hotter rendering the ion-electron Coulomb collisions weaker. However, the electrons cool down via processes like bremsstrahlung, synchrotron emissions etc. keeping their temperature roughly constant upto very inner disc. As a result, while far away from the black hole the flow is in the cooling dominated phase, it transits (or tends to transit) to a radiatively inefficient phase, e.g. ADAF, close to the black hole.

4 DISC FLOWS AROUND SUPERMASSIVE BLACK HOLES

Here we concentrate on two extreme regimes: (1) sub-Eddington limit of accretion with $\dot{M} = 0.01$, which is presumably the case of under-luminous AGNs, (2) super-Eddington accretion with $\dot{M} = 10$, which presumably mimics ultra-luminous quasars and highly luminous AGNs. However, a detailed work of two temperature viscous accretion flows in the possible range of accretion rates: $0.00001 \lesssim \dot{M} \lesssim 100$, around rotating supermassive black holes is under preparation (Rajesh & Mukhopadhyay 2009)

4.1 Sub-Eddington accretors

The under-luminous AGNs and quasars (e.g. Sgr A^*) could be described by the advection dominated model, where the flow is likely to be substantially sub-critical/sub-Eddington with a very low luminosity ($\lesssim 10^{35}$ erg/s). Therefore the present case of $\dot{M} \lesssim 0.01$ could be an appropriate model for describing under-luminous sources. The parameters for the model case described here are given in Table 1.

Naturally the density of the disc around a supermassive black hole is much lower compared to that around a stellar mass black hole. Therefore, the cooling processes, particularly the bremsstrahlung radiation which is only density dependent, become inefficient leading to a high f. However, Fig. 3a shows that the velocity profile is similar to that around a stellar mass black hole. From Fig. 3c we see that $f \to 1$ in most of the sub-Keplerian regime. Close to the black hole there is a possible convective instability as shown in Fig. 3d. This is due to a strong advection of matter.

Figure 4 shows the variation of cooling processes and the corresponding temperature profiles with the radial coordinate. A low $\dot{M}$ corresponds to a radiatively inefficient hot two temperature Keplerian-sub-Keplerian transition region. However, a point to be noted is that unlike stellar mass black holes, only the bremsstrahlung radiation is effective in cooling the flow around a supermassive black hole. This is due to a low magnetic field in the disc around a supermassive black hole rendering synchrotron radiation insignificant.

4.2 Super-Eddington accretors

The highly luminous AGNs and ultra-luminous quasars with radio jet (e.g. PKS 0743-67; Punsly & Tingay 2005), possibly in ULIRGs (Genzel et al. 1998) and narrow-line Seyfert 1 galaxies (e.g. Mineshige et al. 2000), are likely to be ultra-luminous accretors with a high kinetic luminosity ($\sim 10^{46} - 10^{49}$ erg/s). Therefore, the parameter set given in the last row of Table 1 could be appropriate to describe such sources.

The basic flow properties (shown in Figs. 5 and 6) are pretty similar to those around stellar mass black holes, except that in the present case the centrifugal barrier smears out, as evident from Fig. 5a. This is due to high black hole mass causing the density of the flow to be low, resulting in a fast infall. This also leads to, unlike that of a stellar mass black hole, an inefficient synchrotron radiation even at the inner edge of the disc. Similar to the stellar mass black hole, the flow transits from a cooling dominated phase to a radiatively inefficient phase during infalling towards the black hole.

5 COMPARISON BETWEEN FLOWS WITH DIFFERENT α

So far we have discussed models with a typical Shakura-Sunyaev viscosity parameter $\alpha = 0.01$. Now we plan to explore a lower α to understand any significant change in the flow properties.

The rate of energy-momentum transfer between any two successive layers of the fluid element naturally decreases for a lower value of α, which increases the residence time of the flow in the sub-Keplerian disc. Moreover, due to inefficiency of the outward transport of angular momentum, a low α can not keep the flow Keplerian below a certain radius, resulting in a larger Keplerian-sub-Keplerian transition radius. Now, as we know, a high residence time of the flow in the disc corresponds to a high probability of cooling. Therefore, the flow with a lower α is expected to be cooler with a small f. In order to compare, we consider the sub-Eddington accretion with $\dot{M} = 0.01$ around a supermassive black hole of mass $M = 10^7$, e.g. Sgr A^*, with $\alpha = 0.0001, 0.01$.

Figure 7 shows that the velocity profile does not change very significantly for $\alpha = 0.0001$ compared to that of $\alpha = 0.01$. However, importantly, the flow is in the cooling dominated single temperature phase at around the transition radius. As it advances fast in the sub-Keplerian part, the efficiency of cooling decreases due to a decrease in the residence time of the flow in the disc rendering a transition to the radiatively inefficient phase, e.g. ADAF, with $f \to 1$. Subsequently, at $x \leq 17$, f goes down again rapidly and reaches zero at $x \sim 10$ (see Fig. 7c). Hence, the transition from the radiatively inefficient ADAF phase to GAAF phase is very sharp. As a consequence the flow remains stable even upto the horizon (see Fig. 7b). As the Keplerian-sub-Keplerian transition region for a low α is far away from the black hole, compared to that of a large α, the gravitational effect is weaker there in the former case. Consequently, T_e and T_p merge before the flow reaches the transition region, unlike in the case of a large α (= 0.01) flow.

6 DISCUSSION AND SUMMARY

We have investigated the two temperature accretion flow around black holes with the self-consistent solutions of the complete set of hydrodynamic equations, appropriate for modeling disc flows, along with cooling processes. We have considered three important cooling processes: bremsstrahlung, synchrotron and inverse-Comptonization due to synchrotron photons. Synchrotron emission is significant when the magnetic field is high, which is particularly the case for a stellar mass black hole.

After solving the complete set of disc equations, we have seen, in several cases, that there is a transition in the flow from ADAF phase to GAAF phase and vice versa. This is easily understood from the cooling efficiency factor f, calculated for each model. Note that we do not impose any restriction to the flow parameters, unlike the previous authors (Narayan & Yi 1994, 1995). While the previous authors especially restricted with flows having $f = 1$, here we do not impose any such restriction to start with and let the parameter f be determined self-consistently as the system evolves. Therefore, our model is very general whose special case may be understood as an ADAF at a particular region of the disc.

We have especially explored optically thin flows incorporating various nonthermal cooling processes. Figure 8 shows the variation of the effective optical depth with disk radii for various cases discussed here. Note that the maximum possible optical depth to be $\sim 10^{-6}$, supporting our choice of optically thin flows strictly.

The present model can also explain the under-luminous to ultra-luminous sources, stellar mass to supermassive black holes. The luminosity of the under-luminous source Sgr A^* can be explained by a model with $\dot{M} \lesssim 0.0001$ and $M = 10^6 - 10^7$. On the other hand $\dot{M} \sim 100$ around a similar black hole can explain the highly luminous AGNs like PKS 0743-67. The observed luminosity of ULX sources can also be well fitted with this kind of high accretion rate, for the stellar mass black hole. The computed luminosity is given in Table 2.

In general, a low mass accretion rate corresponds to a low density, which may lead to weak emission processes with higher f. Hence, for a sub-Eddington flow, f is close to unity, giving radiatively inefficient ADAF, while a super-Eddington flow may lead ultimately to a GAAF phase with $f < 1$. However, with a lower value of α the residence time of matter in the disc increases, which further makes the disc act as a more efficient radiator.

In most of the cases, the ion and electron temperatures merge or tend to merge at around the transition radius. This is because the electrons and ions are in thermal equilibrium and thus virial around the transition radius, particularly at a high $\dot{M}$. As the sub-Keplerian flow advances, the ions become hotter, rendering the ion-electron Coulomb collisions weaker. The electrons, however, cool down via processes like

bremsstrahlung, synchrotron emissions etc., keeping their temperature roughly constant upto very inner part of the disc. This strictly reveals the two temperature nature throughout.

Next, one should try to predict spectra emitted from the accretion flow in the cases of different parameters based on the present solutions. Naturally, unlike the optically thick Shakura-Sunyaev (1973) disk, the spectra corresponding to GAAF should be dominated by non-thermal processes. This will provide important insights into the geometry and physics of emitting regions.

ACKNOWLEDGMENTS

References

Begelman, M. C., King, A. R., & Pringle, J. E. 2006, MNRAS, 370, 399.

Bisnovatyi-Kogan, G. S., & Lovelace, R. V. E. 2000, ApJ, 529, 978.

Chakrabarti, S. K. 1989, ApJ, 347, 365.

Chakrabarti, S. K. 1996, ApJ, 464, 664.

Chakrabarti, S. K., & Titarchuk, L. G. 1995, ApJ, 455, 623.

Eardley, D. M., & Lightman, A. P. 1975, ApJ, 200, 187.

Eggum, G. E., Coroniti, F. V., & Katz, J. I. 1985, ApJ, 298, 41.

Fabbiano, G. 2004, RMxAC, 20, 46.

Fabrika, S. 2004, ASPRv, 12, 1.

Genzel, R., et al. 1998, ApJ, 498, 579.

Ghosh, S., & Mukhopadhyay, B. 2009, RAA, 9, 157.

Lightman, A. P., & Shapiro, S. L. 1975, ApJ, 198, 73.

Lovelace, R. V. E., Romanova, M. M., & Newman, W. I. 1994, ApJ, 437, 136.

Mandal, S., & Chakrabarti, S. K. 2005, A&A, 434, 839.

Matsumoto, R., Kato, S., Fukue, J., & Okazaki, A. T. 1984, PASJ, 36, 71.

Melia, F., & Misra, R. 1993, ApJ, 411, 797.

Mineshige, S., Kawaguchi, T., Takeuchi, M., & Hayashida, K. 2000, PASJ, 52, 499.

Muchotrzeb, B., & Paczynski, B. 1982, AcA, 32, 1.

Mukhopadhyay, B. 2002, ApJ, 581, 427.

Mukhopadhyay, B. 2003, ApJ, 586, 1268.

Mukhopadhyay, B., & Ghosh, S. 2003, MNRAS, 342, 274; MG03.

Narayan, R., Igumenshchev, I. V., & Abramowicz, M. A. 2000, ApJ, 539, 798.

Narayan, R., & Popham, R. 1993, Nature, 362, 820.

Narayan, R., & Yi, I. 1994, ApJ, 428, 13.

Narayan, R., & Yi, I. 1995, ApJ, 452, 710.

Novikov, I. D., & Thorne, K. S. 1973, in Black Holes, Les Houches 1972 (France), ed. B. & C. DeWitt (New York: Gordon & Breach), 343.

Pringle, J. E., & Rees, M. J. 1972, A&A, 21, 1.

Punsly, B., & Tingay, S. J. 2005, ApJ, 633, 89.

Quataert, E., & Gruzinov, A. 2000, ApJ, 539, 809.

Rajesh, S. R., & Mukhopadhyay, B. 2009, MNRAS (to appear).

Shakura, N., & Sunyaev, R. 1973, A&A, 24, 337.

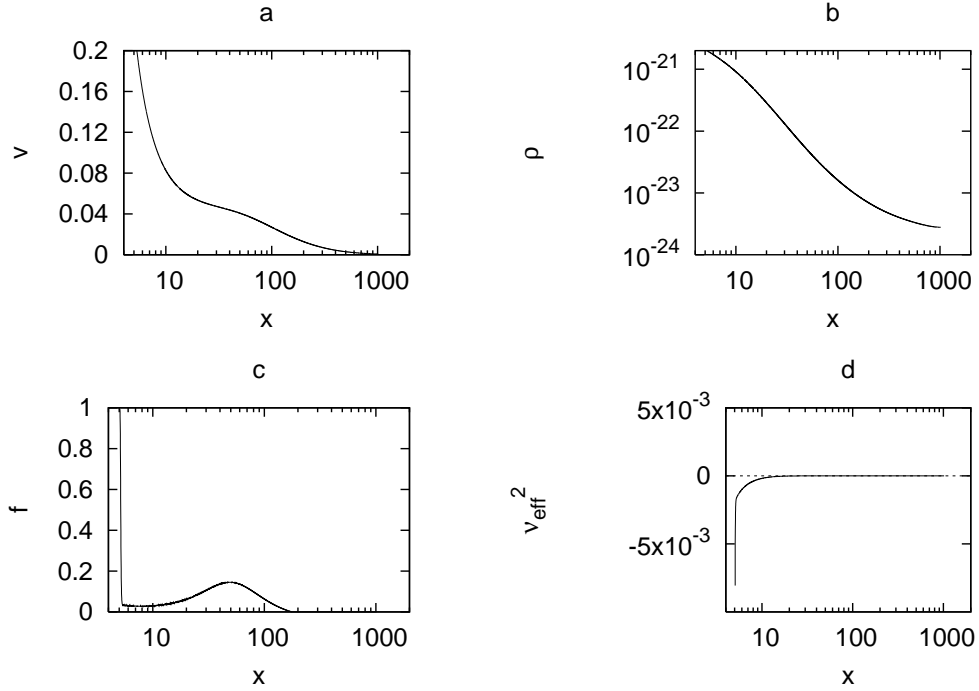Shapiro, S. L., Lightman, A. P., & Eardley, D. M. 1976, ApJ, 204, 187.

Fig. 1 Variation of dimensionless (a) radial velocity, (b) density, (c) cooling factor, (d) square of convective frequency, as functions of radial coordinate for $\dot{M} = 10$. Other parameters are $\alpha = 0.01$, $M = 10$, $\gamma = 1.345$; see Table 1 for details.

Table 1: Parameters for $\alpha = 0.01$, $a = 0$, when the subscript 'c' indicates the quantity at the sonic radius and T_{ec} is expressed in units of $m_i c^2 / k$

M	$\dot{M}$	γ	x_c	λ_c	T_{ec}
10	10	1.345	5.5	3.2	0.000181565
10^7	0.01	1.5	5.5	3.2	0.0001
10^7	10	1.345	5.5	3.2	0.000427

Table 2: Luminosity in erg/sec

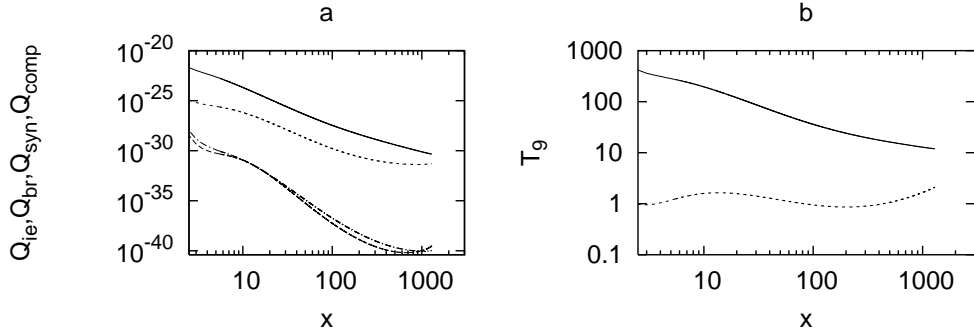| M	$\dot{M}$	γ	L
10^7	0.0001	1.6	10^{34}
10^7	100	1.34	10^{47}
10	100	1.34	10^{40}
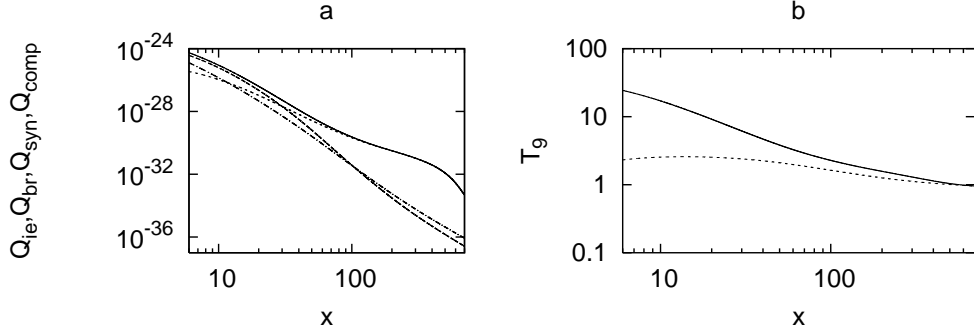
Fig. 2 Variation of (a) dimensionless energy of Coulomb coupling (solid line), bremsstrahlung (dotted line), synchrotron (dash-dotted line), inverse Comptonization due to synchrotron photon (dashed line) processes in logarithmic scale, (b) corresponding ion (solid) and electron (dotted) temperatures in units of 10^9K, as functions of radial coordinate for $\dot{M} = 10$. Other parameters are $\alpha = 0.01$, $M = 10$, $\gamma = 1.345$; see Table 1 for details.
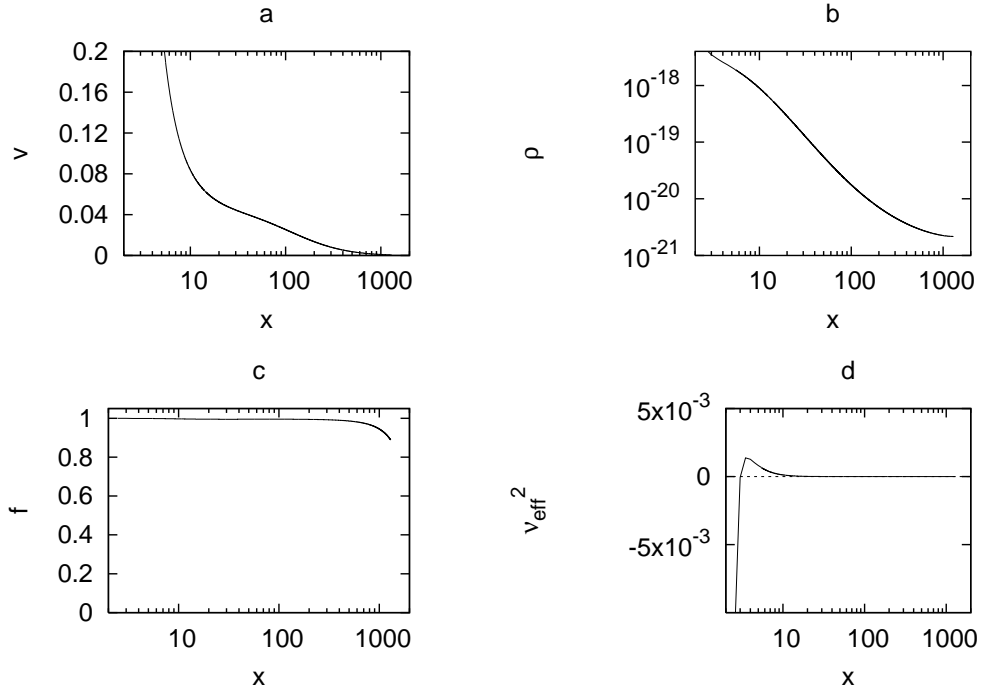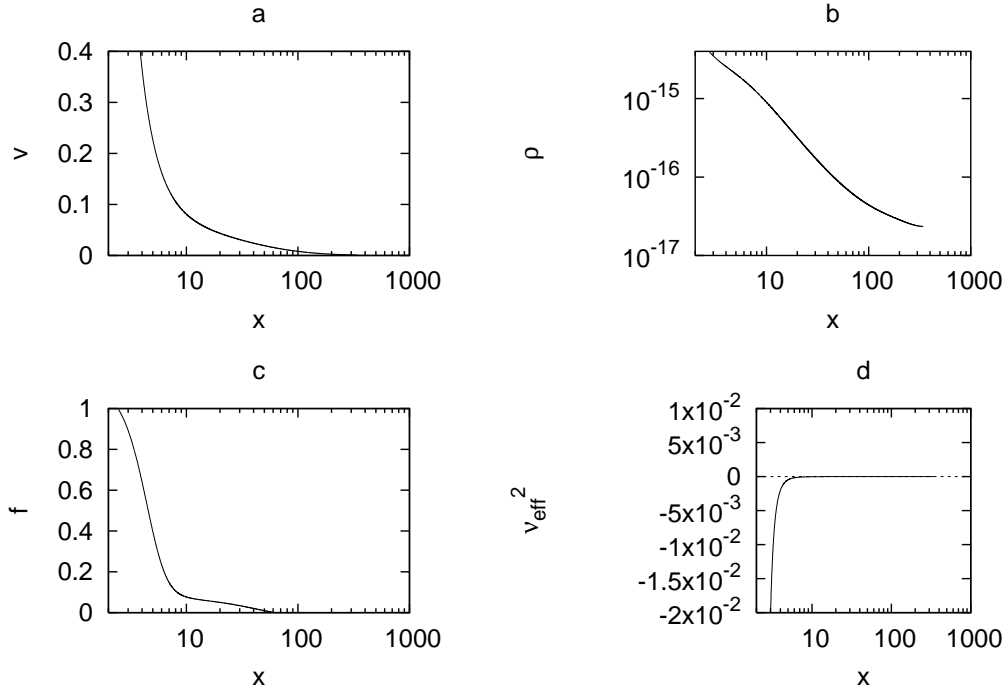

Fig. 3 Variation of dimensionless (a) radial velocity, (b) density, (c) cooling factor, (d) square of convective frequency, as functions of radial coordinate for $\dot{M} = 0.01$. Other parameters are $\alpha = 0.01$, $M = 10^7$, $\gamma = 1.5$; see Table 1 for details.
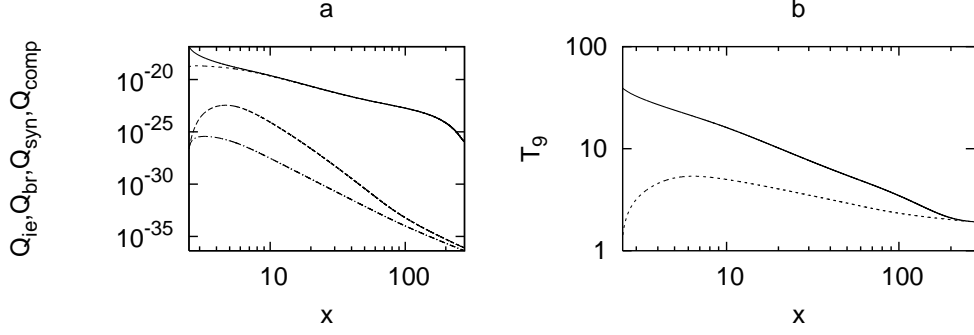
Fig. 4 Variation of (a) dimensionless energy of Coulomb coupling (solid line), bremsstrahlung (dotted line), synchrotron (dash-dotted line), inverse Comptonization due to synchrotron photon (dashed line) processes in logarithmic scale, (b) corresponding ion (solid) and electron (dotted) temperatures in units of 10^9K, as functions of radial coordinate for $\dot{M} = 0.01$. Other parameters are $\alpha = 0.01$, $M = 10^7$, $\gamma = 1.5$; see Table 1 for details.

Fig. 5 Variation of dimensionless (a) radial velocity, (b) density, (c) cooling factor, (d) square of convective frequency, as functions of radial coordinate for $\dot{M} = 10$. Other parameters are $\alpha = 0.01$, $M = 10^7$, $\gamma = 1.345$; see Table 1 for details.

Fig. 6 Variation of (a) dimensionless energy of Coulomb coupling (solid line), bremsstrahlung (dotted line), synchrotron (dash-dotted line), inverse Comptonization due to synchrotron photon (dashed line) processes in logarithmic scale, (b) corresponding ion (solid) and electron (dotted) temperatures in units of 10^9 K, as functions of radial coordinate for $\dot{M} = 10$. Other parameters are $\alpha = 0.01$, $M = 10^7$, $\gamma = 1.345$; see Table 1 for details.
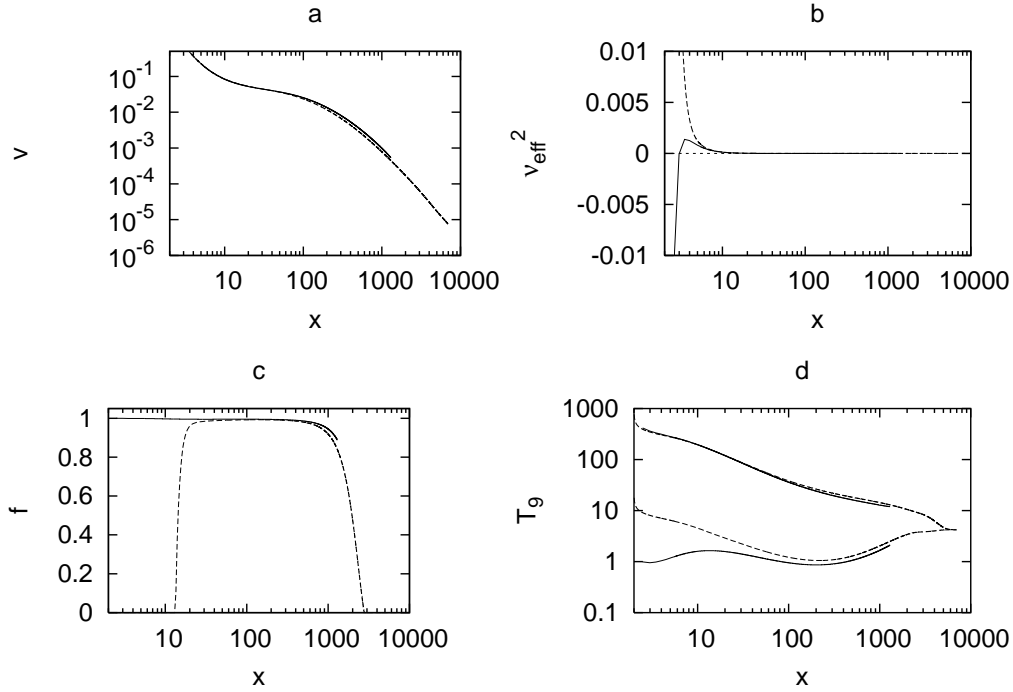

Fig. 7 Comparison between solutions for high and low α: Variation of dimensionless (a) velocity, (b) square of convective frequency, (c) cooling factor, (d) ion (upper set of lines) and electron (lower set of lines) temperatures, a functions of radial coordinate, when solid lines correspond to $\alpha = 0.01$ and dashed lines correspond to $\alpha = 0.0001$. Other parameters are $\dot{M} = 0.01$, $M = 10^7$, $\gamma = 1.5$, $a = 0$.
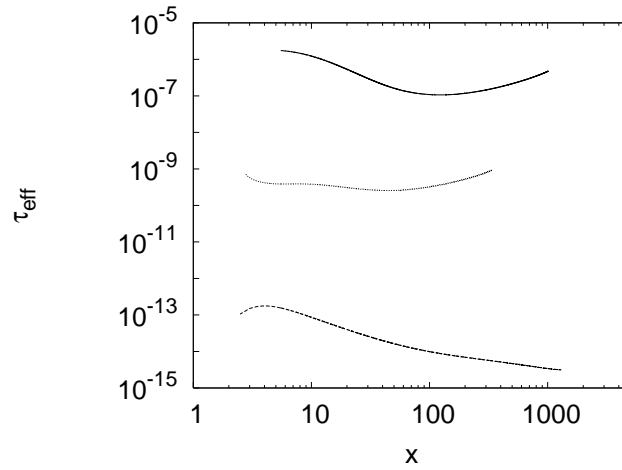
Fig. 8   Variation of the effective optical depth as a function of radial coordinate for the model cases given in Table 1. Solid and dotted curves correspond to stellar and supermassive black holes with super-Eddington accretion rate and dashed curve corresponds to supermassive black hole with sub-Eddington accretion rate. See Table 1 for details.